Aerial Grasping of a Moving Target with a Quadrotor UAV

Riccardo Spica, Antonio Franchi, Giuseppe Oriolo, Heinrich H. Bülthoff, Paolo Robuffo Giordano

Abstract— For a quadrotor aircraft, we study the problem of planning a trajectory that connects two arbitrary states while allowing the UAV to grasp a moving target at some intermediate time. To this end, two classes of canonical grasping maneuvers are defined and characterized. A planning strategy relying on differential flatness is then proposed to concatenate one or more grasping maneuvers by means of spline-based subtrajectories, with the additional objective of minimizing the total transfer time. The proposed planning algorithm is not restricted to pure hovering-to-hovering motions and takes into account practical constraints, such as the finite duration of the grasping phase. The effectiveness of the proposed approach is shown by means of physically-based simulations.

I. INTRODUCTION

Small-scale Unmanned Aerial Vehicles (UAVs) are popular robotic platforms because of their low cost, versatility and simplicity of use [1]. In addition to their usual applications (e.g., aerial monitoring [2], teleoperation [3], and network connectivity [4]), quadrotor UAVs have also recently proven to be an effective platform for aerial manipulation, transportation and assembly tasks [5], [6], [7], [8], [9]. Motivated by these emerging research directions, in this paper we address the problem of trajectory planning for a quadrotor UAV that must grasp a moving object with an onboard gripper while coping with limited actuation authority.

Several planning strategies have been recently proposed for performing pure motion tasks (no intermediate grasping) with quadrotor UAVs. In [10], [11], [12], the trajectories are parameterized using polynomials or splines, and the optimal values of the parameters are obtained by resorting to numerical methods. Pontryagin's maximum principle for a simplified quadrotor model is used in [13], [14]. All these approaches either assume *hovering* initial and final states [11], [12], [13], or do not allow to specify the full initial and/or final state (for instance, in [10] the final state is not fully specified, while in [14] the yaw dynamics is neglected). This may be a practical limitation, e.g., when a particular application requires fast switching between consecutive grasping phases that should be performed 'on-the-fly'.

The hovering requirement is relaxed in [15], in which the quadrotor, after having reached a suitable launch configu-

ration during a preliminary phase, switches to an attitude-only controller in order to steer its trajectory towards the desired final pose in a quasi-open-loop fashion. However, this approach requires an experimental trial-and-error procedure to be performed in advance. This heuristic step is crucial in order to find the appropriate launch configuration and control parameters that will guarantee acceptable final position accuracy for the quadrotor.

As for UAV applications focusing on grasping tasks, some solutions have been explored in the recent literature. Control of a gripping mechanism with compensation of the payload effects on the system dynamics is presented in [16]. In [17], several issues are explored related to automatic assembly and construction of structures using flying vehicles. In both these works the object to be grasped is assumed to be stationary, and grasping is performed in hovering conditions. Hence, the problem is essentially reduced to planning a rectilinear point-to-point motion without specific optimality concerns.

With respect to the state of the art, the contributions of this paper can be summarized as follows: i) we explicitly consider the duration of the trajectory in order to minimize it; ii) we allow the quadrotor to attain generic, and in particular non-hovering, states for starting and ending the grasping phase; iii) we take into account the fact that the target is moving; iv) we include additional practical constraints such as limited actuation capabilities and the requirement of a finite time to actually lock the gripper and perform the grasp. Although the main focus is on the planning stage, we also discuss how to implement our proposed strategy by closed-loop tracking control for the quadrotor motion (thus, not relying on temporary open-loop phases as done in [15]).

The paper is organized as follows. After a formal definition of the problem in Sec. II, in Secs. III and IV we propose two classes of grasping trajectories and discuss how to determine, within these classes, a time-optimal solution for connecting generic initial and final states. In Sec. V we report physically-realistic simulation results illustrating the performance of our method, and we offer some concluding remarks in Sec. VI.

II. AERIAL GRASPING PROBLEM

Denote with $\mathcal{W} : \{O_W; \boldsymbol{x}_W, \boldsymbol{y}_W, \boldsymbol{z}_W\}$ the world inertial frame and with $\mathcal{B} : \{O_B; \boldsymbol{x}_B, \boldsymbol{y}_B, \boldsymbol{z}_B\}$ the body frame of the UAV with origin at its center of mass. The quadrotor state $\boldsymbol{\chi}$ consists of the position $^{\mathcal{W}}\boldsymbol{r}_B \in \mathbb{R}^3$, linear velocity $^{\mathcal{W}}\dot{\boldsymbol{r}}_B \in \mathbb{R}^3$, orientation $^{\mathcal{W}}\boldsymbol{R}_B \in SO(3)$ and angular velocity $^{\mathcal{B}}\boldsymbol{\omega}_{BW} \in \mathbb{R}^3$ of $\mathcal{B}$ w.r.t. $\mathcal{W}$, with the latter angular velocity being expressed for convenience in the body frame $\mathcal{B}$. In the next, we will omit the left superscript whenever quantities are assumed to be expressed in the world frame $\mathcal{W}$.

R. Spica, A. Franchi and P. Robuffo Giordano are with the Max Planck Institute for Biological Cybernetics, Spemannstraße 38, 72076 Tübingen, Germany. E-mail: `riccardo.spica@gmail.com`, {`antonio.franchi`, `prg`}`@tuebingen.mpg.de`.

G. Oriolo is with the Dipartimento di Ingegneria Informatica, Automatica e Gestionale, Università di Roma La Sapienza, Roma, Italy. E-mail: `oriolo@dis.uniroma1.it`

H. H. Bülthoff is with the Max Planck Institute for Biological Cybernetics, Spemannstraße 38, 72076 Tübingen, Germany, and with the Department of Brain and Cognitive Engineering, Korea University, Seoul, 136-713 Korea. E-mail: `hhb@tuebingen.mpg.de`.

As well known [18], each of the four propellers produces a force F_i and a torque M_i along and about $\boldsymbol{z}_\mathcal{B}$, respectively, and both proportional to the square of the propeller rotational speeds ω_i:

$$F_i = k_F \omega_i^2, \qquad M_i = k_M \omega_i^2, \qquad k_F > 0,\, k_M > 0.$$

As usually done, we consider the motors dynamics to be fast enough compared to the quadrotor dynamics, and take the square of the 4 rotational speeds $\tilde{\boldsymbol{u}} = (\omega_1^2 \;\; \omega_2^2 \;\; \omega_3^2 \;\; \omega_4^2)^T$ as actual control inputs. The following linear input transformation maps the individual propeller forces and torques to the total thrust $u_1 \in \mathbb{R}$ along $\boldsymbol{z}_\mathcal{B}$ and torques $(u_2, u_3, u_3)^T \in \mathbb{R}^3$ about $\boldsymbol{x}_\mathcal{B}$, $\boldsymbol{y}_\mathcal{B}$ and $\boldsymbol{z}_\mathcal{B}$ applied to the quadrotor body:

$$\boldsymbol{u} = \begin{pmatrix} u_1 \\ u_2 \\ u_3 \\ u_4 \end{pmatrix} = \begin{pmatrix} k_F & k_F & k_F & k_F \\ 0 & k_F l & 0 & -k_F l \\ -k_F l & 0 & k_F l & 0 \\ k_M & -k_M & k_M & -k_M \end{pmatrix} \tilde{\boldsymbol{u}} = \boldsymbol{A}\tilde{\boldsymbol{u}}, \tag{1}$$

where l is the distance from the rotor axes of rotation to the quadrotor center and the square matrix $\boldsymbol{A}$ is always nonsingular.

The translational dynamics of the quadrotor is then described by

$$m\ddot{\boldsymbol{r}}_\mathcal{B} = -mg\boldsymbol{e}_3 + u_1 \boldsymbol{z}_\mathcal{B}, \tag{2}$$

where $\boldsymbol{e}_3$ represents the world-frame vertical direction, and m the total mass of the robot. Similarly, the rotational dynamics obeys

$$\mathcal{J}\,{}^\mathcal{B}\dot{\boldsymbol{\omega}}_{\mathcal{B}\mathcal{W}} + {}^\mathcal{B}\boldsymbol{\omega}_{\mathcal{B}\mathcal{W}} \times \mathcal{J}\,{}^\mathcal{B}\boldsymbol{\omega}_{\mathcal{B}\mathcal{W}} = \begin{pmatrix} u_2 \\ u_3 \\ u_4 \end{pmatrix}, \tag{3}$$

where $\mathcal{J}$ is the constant inertia matrix expressed in the body frame $\mathcal{B}$.

Consider now a gripper rigidly attached to the quadrotor and with an associated frame $\mathcal{G} : \{O_\mathcal{G};\; \boldsymbol{x}_\mathcal{G};\; \boldsymbol{y}_\mathcal{G};\; \boldsymbol{z}_\mathcal{G}\}$ having a constant position ${}^\mathcal{B}\boldsymbol{r}_\mathcal{G}$ and orientation ${}^\mathcal{B}\boldsymbol{R}_\mathcal{G}$ w.r.t. $\mathcal{B}$. We assume that either the mass of the gripper is negligible w.r.t. the UAV, or that some counterweighting mechanism is exploited to compensate for the effect of the gripper mass on the overall barycenter position. This assumption allows us to take (2-3) as a good approximation of the quadrotor/gripper dynamics. Finally, we consider, for the sake of realism, a gripper needing a *finite* time $T_g^{\min} > 0$ in order to actually grasp the target. The following (straightforward) relationship is useful for the next developments

$$\dot{\boldsymbol{r}}_\mathcal{G} = \dot{\boldsymbol{r}}_\mathcal{B} + {}^\mathcal{W}\boldsymbol{R}_\mathcal{B}\left({}^\mathcal{B}\boldsymbol{\omega}_{\mathcal{B}\mathcal{W}} \times {}^\mathcal{B}\boldsymbol{r}_\mathcal{G}\right). \tag{4}$$

We also denote with (α, β, ρ) the spherical coordinates (i.e., azimuth, zenith distance, and radius) of $O_\mathcal{G}$ w.r.t. $\mathcal{B}$.

The target to be grasped is modeled as a rigid body moving along a known three-dimensional trajectory with a constant velocity phase[1] of at least $T_g^{\min}$. We let $\mathcal{T} : \{O_\mathcal{T} :$
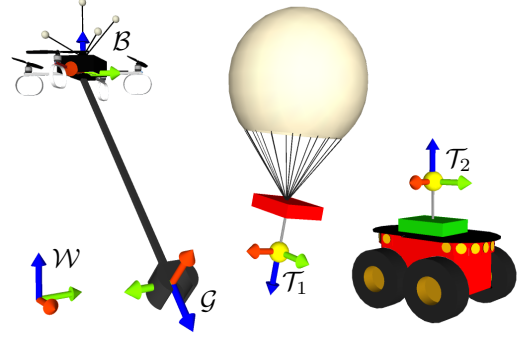
Fig. 1: Reference frames involved in the aerial grasping: $\mathcal{T}_1$ and $\mathcal{T}_2$ refer to a airborne and a ground-transported target, respectively.

$\boldsymbol{x}_\mathcal{T}, \boldsymbol{y}_\mathcal{T}, \boldsymbol{z}_\mathcal{T}\}$ be the frame attached to the target, and denote its position $\boldsymbol{r}_\mathcal{T}$ and orientation ${}^\mathcal{W}\boldsymbol{R}_\mathcal{T}$ w.r.t. the world frame. The target handle is assumed to possess a spherical symmetry in order to neglect the effects of its orientation in space. Figure 1 summarizes in an illustrative way the various frames of interest.

In order for the grasping to be successful, the following constraints must be satisfied for all $t \in [t_g,\, t_g + T_g^{\min}]$, where t_g represents the starting time of the grasping phase.

Constraint 1. *The position and velocity of $O_\mathcal{G}$ (the center of grasping) must match those of $O_\mathcal{T}$, that is:*

$$\boldsymbol{r}_\mathcal{G}(t) = \boldsymbol{r}_\mathcal{B}(t) + {}^\mathcal{W}\boldsymbol{R}_\mathcal{B}(t)\,{}^\mathcal{B}\boldsymbol{r}_\mathcal{G} = \boldsymbol{r}_\mathcal{T}(t) \tag{5}$$

$$\dot{\boldsymbol{r}}_\mathcal{G}(t) = \dot{\boldsymbol{r}}_\mathcal{B}(t) + {}^\mathcal{W}\boldsymbol{R}_\mathcal{B}(t)\left({}^\mathcal{B}\boldsymbol{\omega}_{\mathcal{B}\mathcal{W}}(t) \times {}^\mathcal{B}\boldsymbol{r}_\mathcal{G}\right) = \dot{\boldsymbol{r}}_\mathcal{T}(t). \tag{6}$$

Note that, using (5), (6) implies that

$$\dot{\boldsymbol{r}}_\mathcal{B}(t) = \dot{\boldsymbol{r}}_\mathcal{T}(t) + {}^\mathcal{W}\boldsymbol{R}_\mathcal{B}(t)\,{}^\mathcal{B}\boldsymbol{\omega}_{\mathcal{B}\mathcal{W}}(t) \times (\boldsymbol{r}_\mathcal{B}(t) - \boldsymbol{r}_\mathcal{T}(t)) \tag{7}$$

must hold $\forall t \in [t_g,\, t_g + T_g^{\min}]$. It is worth noting that, during the grasping, this constraint still allows for a quadrotor rotation around the target with an angular velocity ${}^\mathcal{B}\boldsymbol{\omega}_{\mathcal{B}\mathcal{W}}$, with the particular case ${}^\mathcal{B}\boldsymbol{\omega}_{\mathcal{B}\mathcal{W}} = 0$ describing a hovering grasp.

In addition to the grasping constraint, we also impose the following actuation constraint:

Constraint 2. *The propeller angular speed are bounded:*

$$\tilde{\boldsymbol{u}} \in \tilde{U} = [\underline{\omega}, \overline{\omega}] \times [\underline{\omega}, \overline{\omega}] \times [\underline{\omega}, \overline{\omega}] \times [\underline{\omega}, \overline{\omega}], \tag{8}$$

with $0 < \underline{\omega} < \overline{\omega}$.

Constraint 2 can be mapped into the space of admissible transformed inputs through (1):

$$\boldsymbol{u} \in U = \left\{\boldsymbol{u} \in \mathbb{R}^4 : \boldsymbol{u} = \boldsymbol{A}\tilde{\boldsymbol{u}} \text{ where } \tilde{\boldsymbol{u}} \in \tilde{U}\right\}.$$

It is easy to verify that, because of the shape of matrix $\boldsymbol{A}$ and of Constraint 2, the thrust input u_1 is bound to be positive at all times.

Letting $X_g(t)$ be the set of quadrotor states $\boldsymbol{\chi}$ for which the grasping is admissible at some given time t, i.e., such that (5) and (6) hold at t, we then state our generic grasping problem as:
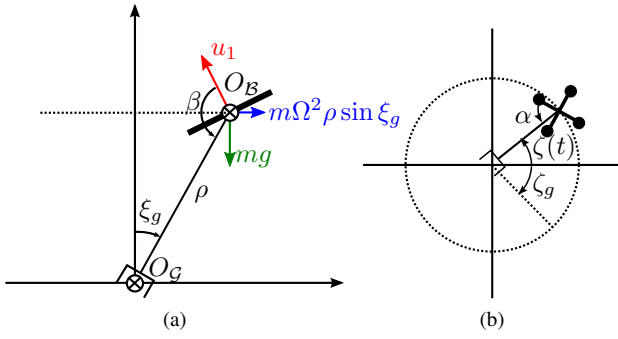
Fig. 2: Side (a) and top (b) views of the horizontal gripper-closure subtrajectory (Class I), with forces and relevant parameters. Note that ξ_g is constant in this case, while $\zeta(t) = \Omega(t - t_g) + \zeta_g$ is a time-varying quantities starting from the initial value $\zeta(t_g) = \zeta_g$.
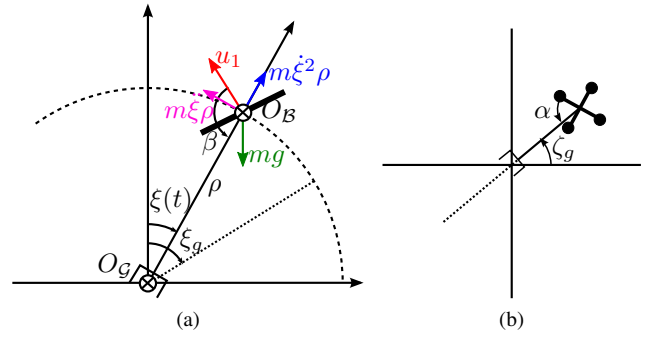

Fig. 3: Side (a) and top (b) views of the vertical gripper-closure subtrajectory (Class II), with forces and relevant parameters. Note that, contrarily to the previous case, here ζ_g is a constant parameter, while $\xi(t)$ and $\dot{\xi}(t)$ change over time with initial values $\xi_g, \dot{\xi}_g$.

Problem 1. *Given an initial quadrotor state $\boldsymbol{\chi}_i$, an initial time t_i and a final state $\boldsymbol{\chi}_f$, find a feasible trajectory $\boldsymbol{\chi}^*(t) : [t_i, t_f] \rightarrow SE(3) \times se(3)$ traveling from $\boldsymbol{\chi}_i$ to $\boldsymbol{\chi}_f$ that minimizes the travel time $t_f - t_i$, and lets the UAV perform the grasping during some intermediate time interval $[t_g, t_g + T_g^{\min}] \subset [t_i, t_f]$ (with t_g to be determined). More formally, find a $\boldsymbol{\chi}^*(t)$ that solves the following minimization problem*

$$\min_{\{\boldsymbol{\chi}^*, t_g, t_f\}} t_f - t_i$$

s.t. $\boldsymbol{\chi}^*(t_i) = \boldsymbol{\chi}_i$, $\boldsymbol{\chi}^*(t_f) = \boldsymbol{\chi}_f$, $\boldsymbol{\chi}^*(t) \in X_g(t) \ \forall t \in [t_g, t_g + T_g^{\min}] \subset [t_i, t_f]$, $\boldsymbol{u} \in U$, and $\boldsymbol{\chi}$ obeys the quadrotor dynamics (2–3).

III. SUBTRAJECTORIES FOR GRIPPER CLOSURE

In order to render the proposed minimization problem more tractable, we characterize and analyze in detail two distinct classes of feasible trajectories for which Constraint 1 can be continuously satisfied inside the time interval in which the target trajectory keeps a constant velocity. Specifically, we present two possible classes of trajectories satisfying this constraint, namely the *horizontal circular class* (Class I) and the *vertical circular class* (Class II). These will form the basis of the search space explored by the optimization procedure discussed in Sec. IV[2]. Note that both classes include the hovering trajectories as particular subcases. In the following we denote with (ζ, ξ, ρ) the spherical coordinates of $O_{\mathcal{B}}$ in a frame parallel to $\mathcal{W}$ and with origin in $O_{\mathcal{T}}$, see Figs. 2 and 3.

A. Class I: Horizontal Circular Trajectories

Consider the class of trajectories in which the quadrotor: i) rotates with constant angular speed $\dot{\zeta} = \Omega$ about a vertical axis parallel to $z_{\mathcal{W}}$ and passing through $O_{\mathcal{T}}$, ii) keeps the zenith distance ξ constant at some given value ξ_g, and iii) has a certain azimuth at t_g, i.e., $\zeta(t_g) = \zeta_g$ (see Fig. 2).

---

[2]These two classes do not characterize the complete set of admissible trajectories continuously satisfying Constraint 1. Nevertheless, they represent a 'functional basis' which can be used to span more complex admissible trajectories by exploiting their complementarity.

The analytical relationship describing such a trajectory can be easily obtained by imposing that the position and velocity of $O_{\mathcal{G}}$ coincide with those of $O_{\mathcal{T}}$, and that the quadrotor control forces compensate gravity and centrifugal forces, as depicted in Fig. 2. In particular, we obtain

$$u_1 = -\frac{mg}{\cos(\xi_g + \beta)}, \tag{9}$$

for the thrust module, and

$$\Omega = \pm\sqrt{\frac{-g\tan(\xi_g + \beta)}{\rho\sin\xi_g}}, \tag{10}$$

for the angular speed Ω. Since (10) constrains the values of ξ_g and Ω, only one among these two quantities can be freely assigned. In this work, we chose to parametrize the Class I of subtrajectories with the quantities ξ_g, $\text{sign}\,\Omega$, ζ_g, the initial position of the target $\boldsymbol{r}_{\mathcal{T}}(t_g)$, and the constant target velocity during the grasping $\dot{\boldsymbol{r}}_{\mathcal{T}}(t_g)$.

The quadrotor torque inputs required to track these trajectories can be obtained by noting that the quadrotor angular acceleration must be null in this case, and by then applying (3). The general expression can be found in [19]. Here, for conciseness, we only report the resulting expression for the case of a symmetric quadrotor ($J_{xx} = J_{yy}$), i.e.,

$$\begin{pmatrix} u_2 \\ u_3 \\ u_4 \end{pmatrix} = \frac{\Omega^2}{2} s_{2\xi_g + 2\beta} (J_{xx} - J_{zz}) \begin{pmatrix} -s_\alpha \\ c_\alpha \\ 0 \end{pmatrix}, \tag{11}$$

where $s = \sin$ and $c = \cos$. Finally, applying (1), we obtain the propeller speeds needed to track a trajectory in Class I:

$$\begin{pmatrix} \omega_1^2 \\ \omega_2^2 \\ \omega_3^2 \\ \omega_4^2 \end{pmatrix} = \begin{pmatrix} -\frac{mg}{4k_F c_{\xi_g+\beta}} - \frac{\Omega^2}{4}\frac{c_\alpha s_{2\xi_g+2\beta}(J_{xx}-J_{zz})}{k_F l} \\ -\frac{mg}{4k_F c_{\xi_g+\beta}} - \frac{\Omega^2}{4}\frac{s_\alpha s_{2\xi_g+2\beta}(J_{xx}-J_{zz})}{k_F l} \\ -\frac{mg}{4k_F c_{\xi_g+\beta}} + \frac{\Omega^2}{4}\frac{c_\alpha s_{2\xi_g+2\beta}(J_{xx}-J_{zz})}{k_F l} \\ -\frac{mg}{4k_F c_{\xi_g+\beta}} + \frac{\Omega^2}{4}\frac{s_\alpha s_{2\xi_g+2\beta}(J_{xx}-J_{zz})}{k_F l} \end{pmatrix}. \tag{12}$$

B. Class II: Vertical Circular Trajectories

In the trajectories belonging to Class II, the quadrotor: i) rotates with an angular speed $\dot{\xi}(t)$ about a horizontal axis orthogonal to $z_{\mathcal{W}}$ and passing through $O_{\mathcal{T}}$, and ii) keeps

$O_{\mathcal{B}}$ inside the plane passing through $O_{\mathcal{T}}$ and orthogonal to the chosen rotation axis (see Fig. 3). Class II represents a complementary set w.r.t. Class I: in fact, in this case $\zeta = \zeta_g$ is constant and $\xi = \xi(t)$ is time-varying as opposite to the previous case.

The analytical expression of a generic trajectory in Class II can be easily obtained by imposing that the position and velocity of $O_{\mathcal{G}}$ coincide with those of $O_{\mathcal{T}}$, and that, again, the quadrotor control forces compensate for gravity and centrifugal forces. However, as additional requirement, for all non-hovering cases the control forces must also generate the tangential acceleration required to produce the needed change of $\dot{\xi}(t)$ over time. Indeed, after some manipulations (available in [19]), one obtains the following differential equation governing the evolution of $\xi(t)$:

$$\rho\left(\dot{\xi}^2 \sin\beta + \ddot{\xi}\cos\beta\right) - g\sin(\xi + \beta) = 0 \qquad (13)$$

with the associated initial conditions at t_g: $\xi(t_g) = \xi_g$ and $\dot{\xi}(t_g) = \dot{\xi}_g$. Consequently, the trajectories of Class II can be parametrized by the constant azimuth ζ_g, the initial values ξ_g, and $\dot{\xi}_g$, and (as for Class I) the initial position of the target $\boldsymbol{r}_{\mathcal{T}}(t_g)$ and the constant target velocity during the grasping $\dot{\boldsymbol{r}}_{\mathcal{T}}(t_g)$. Furthermore, using (13), one can prove that a constant angular velocity ($\ddot{\xi} = 0$) does not represent a feasible solution for this class of trajectory apart for the special hovering case for which $\dot{\xi} \equiv \ddot{\xi} \equiv 0$ at all times.

As for the quadrotor inputs needed to track a Class II trajectory, one has

$$u_1 = m\rho\left(\dot{\xi}^2\cos\beta - \ddot{\xi}\sin\beta\right) - mg\cos(\xi + \beta).$$

Similarly to before, a general expression for the torque inputs can also be obtained after some long but straightforward manipulations. Here, for conciseness, we only report the expression for a symmetric quadrotor

$$\begin{pmatrix} u_2 \\ u_3 \\ u_4 \end{pmatrix} = \ddot{\xi} J_{xx} \begin{pmatrix} s_\beta \\ -c_\beta \\ 0 \end{pmatrix}. \qquad (14)$$

Finally, the required squared motors velocities are:

$$\begin{pmatrix} \omega_1^2 \\ \omega_2^2 \\ \omega_3^2 \\ \omega_4^2 \end{pmatrix} = \begin{pmatrix} \frac{u_1(\xi)}{4k_F} + \frac{\ddot{\xi}c_\beta J_{xx}}{2k_F l} \\ \frac{u_1(\xi)}{4k_F} + \frac{\ddot{\xi}s_\beta J_{xx}}{2k_F l} \\ \frac{u_1(\xi)}{4k_F} - \frac{\ddot{\xi}c_\beta J_{xx}}{2k_F l} \\ \frac{u_1(\xi)}{4k_F} - \frac{\ddot{\xi}s_\beta J_{xx}}{2k_F l} \end{pmatrix}. \qquad (15)$$

C. Gripper Position and Trajectory Parameters

We now analyze how the positioning of the gripper in the quadrotor body frame, described by the quantities (α, β, ρ), affects the attainable horizontal and vertical circular trajectories in terms of the admissible values of the trajectory parameters. One can immediately note that no special restrictions are present on ζ_g and on the particular target position/velocity. Therefore, we focus our analysis on the admissible values of the quantities $\xi_g, \dot{\xi}_g$ for the two classes under consideration.
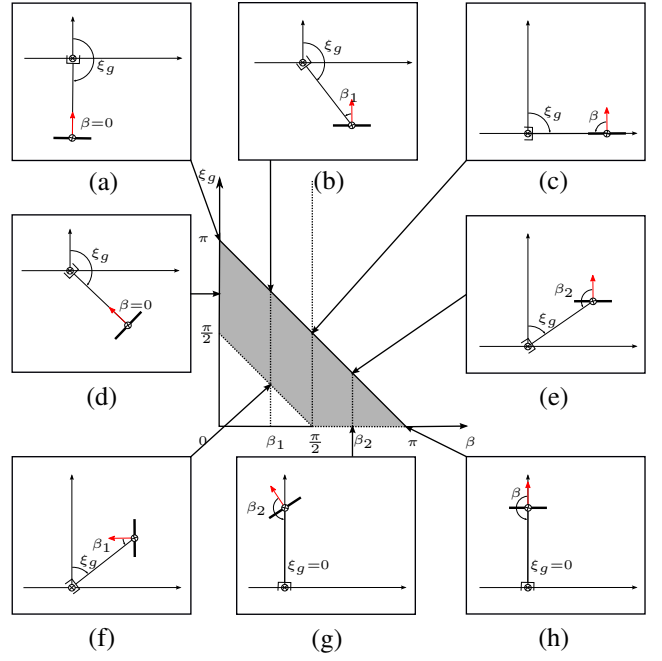

Fig. 4: Admissible values for ξ_g depending on β.

1) Admissible values of ξ_g for Class I: From (9), note that $\cos(\xi_g + \beta) < 0$ for having a positive thrust, and $\tan(\xi_g + \beta) \leq 0$ for Ω to be real (note that $\sin\xi_g \geq 0$). Therefore, the only admissible interval is $\xi_g + \beta \in (\frac{\pi}{2}, \pi]$, implying

$$\xi_g \in \left(\max\left(0, \frac{\pi}{2} - \beta\right), \pi - \beta\right] = (\xi_g^{\mathrm{inf}}, \xi_g^{\mathrm{max}}]. \qquad (16)$$

The results are summarized in Fig. 4 where the admissible set for ξ_g is represented by the gray shaded area. The situation $\xi_g = \xi_g^{\mathrm{max}}$ corresponds to hovering trajectories (see Fig. 4(a-c,e,h)), i.e., $\Omega = 0$, and presents a singularity when $\beta = (0, \pi)$ since Ω becomes undefined (see Fig. 4(a,h)).

Now consider separately the two cases in which the gripper is above or below the quadrotor horizontal plane, i.e., $\beta \in [0, \pi/2)$ or $\beta \in [\pi/2, \pi]$, respectively. The first case yields $\xi_g^{\mathrm{inf}} = \pi/2 - \beta > 0$ making the choice $\xi_g = \xi_g^{\mathrm{inf}}$ unfeasible, as it would imply a perfectly vertical quadrotor with the thrust vector orthogonal to the gravity direction (see, e.g., Fig. 4(f)). In fact, (9) becomes singular in this case. The second case yields $\xi_g^{\mathrm{inf}} = 0$ and $\xi_g = \xi_g^{\mathrm{inf}}$, corresponding to the situation in which $O_{\mathcal{B}}$ is exactly above the target. If $\beta \neq \pi$, this second case is not feasible as it would require an infinite Ω (see (10) and Fig. 4(g)). On the other hand, if $\beta = \pi$ then Ω becomes indefinite, thus corresponding to another hovering situation (see Fig. 4(h)).

It is also clear that values of β too close to π reduce the range of admissible values of ξ_g, and then the number of possible grasping trajectories. In particular, if $\beta = \pi$, it is easy to verify that the sole admissible solutions reduce to the hovering ones.

2) Admissible values of ξ_g and $\dot{\xi}_g$ for Class II: Differently from the previous case, here in general the input u_1 can remain admissible (positive) only for a *finite* time interval whose length depends on β, ρ, ξ_g, and $\dot{\xi}_g$. An explicit
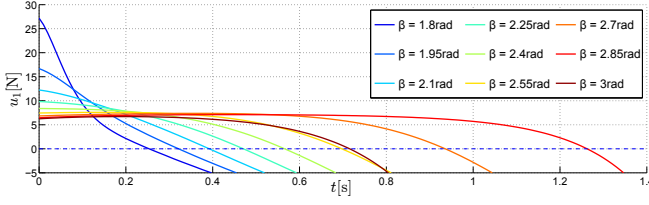
Fig. 5: Thrust evolutions for different β's in a representative case.

expression of this relationship is not available in closed-form since (13) cannot be, in general, integrated analytically. However, we can obtain a qualitative intuition by considering a numerical example. In Fig. 5 we report the time profile of the thrust input obtained by numerical integration of (13) for given ρ, ξ_g, $\dot{\xi}_g$ and several values of β. In this case the maximum duration of the interval where the thrust remains positive is for β around 2.7 rad. Clearly this optimum depends upon the chosen values for ρ, ξ_g, $\dot{\xi}_g$.

D. Final considerations about the role of (α, β, ρ)

The angle α influences the way in which the control effort is distributed among the motors in order to generate the needed torques. For example, from (12) it follows that, when $\alpha = k\frac{\pi}{2}$, only one pair of motors is used to generate the necessary torque. Therefore, in order to guarantee a uniform contribution from every motor (thus reducing the individual motor efforts), a suitable choice is $\alpha = (2k + 1)\frac{\pi}{4}$.

As for β, a value too close to $\pi/2$ might require too high torques in order to sustain the weight of the target. Analogously, a large value of ρ (the gripper length) would also increase the inertia contribution of the target after performing the grasping. Furthermore, the length ρ also determines the angular velocity Ω for a given value of ξ_g, and thus the amount of necessary torques (see (10) and (11)).

Concerning additional possible geometric constraints of the problem, values of β larger or smaller than $\pi/2$ are most suited for ground-transported targets or airborne ones, respectively, see Fig. 1.

IV. TRAJECTORY PLANNING

Our proposed solution for Problem 1 is to generate a trajectory as a composition of 3 sub-trajectories:

1) *Initial transfer:* move from χ_i to a starting state χ_g^i (to be determined) belonging to either a Class I or a Class II gripper-closure trajectory;
2) *Gripper closure:* follow the chosen gripper-closure trajectory for a time interval $T_g \geq T_g^{\min}$;[3]
3) *Final transfer:* move from the final state χ_g^f of the gripper-closure trajectory to χ_f.

We recall that our goal is to find a time-optimal trajectory minimizing the total travel time from χ_i to χ_f. To this end, we execute Algorithm 1 for 3 gripper-closure trajectory cases: Class I with $\Omega \geq 0$, Class I with $\Omega < 0$, and

---

[3]Here, we purposely leave to the optimization the freedom of selecting any $T_g \geq T_g^{\min}$. In fact, despite intuitive considerations, we cannot provide rigorous arguments to conclude the optimality of $T_g = T_g^{\min}$ for all possible situations.

Algorithm 1 Compound trajectory optimization

Require: Gripper-closure trajectory class, χ_i, χ_f, $r_\mathcal{T}$, $\dot{r}_\mathcal{T}$
Require: Initial guesses for ζ_g, ξ_g, T_g (and possibly $\dot{\xi}_g$).
1. **loop**
2.   Compute the gripper-closure trajectory for ζ_g, ξ_g, T_g, ($\dot{\xi}_g$) and the corresponding end-point states χ_g^i, χ_g^f;
3.   Compute a minimum-time initial transfer trajectory from χ_i to χ_g^i and denote its duration with T_i (Algorithm 2);
4.   Compute a minimum-time final transfer trajectory from χ_g^f to χ_f and denote its duration with T_f (Algorithm 2);
5.   Compute the cost function $T_i + T_g + T_f$;
6.   **if** Terminating conditions are satisfied **then**
7.   **return** ζ_g, ξ_g, T_g, ($\dot{\xi}_g$)
8.   **end if**
9.   Select new guesses for ζ_g, ξ_g, T_g, ($\dot{\xi}_g$) ;
10. **end loop**

Class II. The best solution (in terms of minimum time) among these three cases is then selected as the sought optimal trajectory. This decomposition is meant to avoid the introduction of binary variables in the minimization process, as this could negatively affect the performance of gradient-based optimization algorithms.

Note that Algorithm 1 internally makes use of an additional optimization module (defined in Algorithm 2 and described in Sec. IV-B) able to generate feasible transfer trajectories connecting the initial state with the selected gripper-closure trajectory and, symmetrically, the gripper-closure trajectory with the final state. We also stress again that the initial and final states of a gripper-closure trajectory are not bound to be hovering ones. Hovering solutions are anyway part of the search space and could then be returned by Algorithm 1 if found to be optimal.

Before proceeding with the illustration of Algorithm 2, we first discuss the controllability properties of our quadrotor system with *bounded inputs*, since controllability is a prerequisite for the existence of a solution for the optimal control problem under consideration.

A. Controllability between non-hovering states

As already showed in several previous works, the quadrotor dynamics is dynamically feedback linearizable (see, e.g., [18]) and thus differentially flat w.r.t. the flat output $\sigma = \begin{pmatrix} r_\mathcal{B}^T & \psi \end{pmatrix}^T$, where ψ is the yaw angle[4].

A differentially flat system is always controllable in absence of input limitations. Moreover a quadrotor with limited inputs is also controllable if the initial and final states are hovering ones. In fact, it is always possible to uniformly increase the total completion time of the trajectory and, as a consequence, decrease the required control effort until it falls within given limits. This property has been extensively used in the literature for dealing with quadrotors with limited inputs (see, e.g., [12]).

---

[4]A dynamical system is differentially flat if it possible to express its state and inputs as an algebraic explicit function of a flat output σ and a limited number of its derivatives [20]. Output flatness is equivalent to exact dynamic feedback linearizability with the flat output taken as linearizing outputs [21].

Algorithm 2 Transfer trajectory generation

Require: ς_1, ς_2
Require: Initial guess for T (transfer duration).
1. **loop**
2.   Compute the interpolating B-spline for time T;
3.   Compute the constraint function, i.e., the maximum and minimum values of the inputs along the transfer trajectory;
4.   Compute the objective function T;
5.   **if** Conditions for terminating are satisfied **then**
6.   **return** T
7.   **end if**
8.   Select new guess for T;
9. **end loop**

However, the same approach cannot be extended to trajectories connecting non-hovering states as those considered in this work. Nevertheless, by resorting to different arguments, it is still possible to qualitatively prove the controllability of a quadrotor with limited inputs also when considering non-hovering states, as reported in [19].

B. Transfer Trajectory Generation

In addition to characterizing controllability, the quadrotor flatness makes it also possible to move the problem of planning the transfer trajectory from the control input space to the flat output space. Let ς_i, ς_g^i, ς_g^f and ς_f represent the flat output values bijectively associated to the states $\boldsymbol{\chi}_i$, $\boldsymbol{\chi}_g^i$, $\boldsymbol{\chi}_g^f$ and $\boldsymbol{\chi}_f$. The problem then reduces to the planning of a trajectory $\boldsymbol{\sigma}(t)$ for the flat outputs starting at ς_i (ς_g^f) and ending at ς_g^i (ς_f) in a minimum time T_i (T_f) while satisfying Constraint 2.

We express the function $\boldsymbol{\sigma}(t)$ as a linear combination of a certain number of predefined basis functions. Different parametrization techniques have been proposed in the literature differing in the chosen basis. Among the various possibilities, we opted for piecewise polynomials in the B-spline form. To keep the degree of the spline as low as possible, we made use of two different splines: one for the position vector and another (scalar) one for the yaw angle:

$$\boldsymbol{r}_{\mathcal{B}}(t) = \sum_{j=1}^{m_{\boldsymbol{r}_{\mathcal{B}}}} \boldsymbol{p}_{\boldsymbol{r}_{\mathcal{B}},j} B_j^{n_{\boldsymbol{r}_{\mathcal{B}}}}(t), \quad \psi(t) = \sum_{j=1}^{m_{\psi}} p_{\psi,j} B_j^{n_{\psi}}(t),$$

where the coefficients $\boldsymbol{p}_{\boldsymbol{r}_{\mathcal{B}},j}, p_{\psi,j}$ are the B-spline *control points*, $m_{\boldsymbol{r}_{\mathcal{B}}}, m_{\psi}$ represent the number of control points, and $n_{\boldsymbol{r}_{\mathcal{B}}}, n_{\psi}$ the degrees of the splines.

In order to ensure the needed trajectory smoothness required by the quadrotor flatness transformation, we chose $n_{\boldsymbol{r}_{\mathcal{B}}} = 4$ for the position $\boldsymbol{r}_{\mathcal{B}}(t)$ and $n_{\psi} = 2$ for the yaw angle $\psi(t)$, with at least 8 control points for the position ($m_{\boldsymbol{r}_{\mathcal{B}}} = 8$) and of 4 control points for the yaw ($m_{\psi} = 4$). Once the boundary conditions and the total time T are specified, the control points can be easily computed by solving two square linear systems, see [22].

While the boundary conditions are determined by Algorithm 1, optimization of the transfer time T pertains to the inner Algorithm 2 which, at each iteration, solves an instance

of the following problem

$$\min_{\{T>0, \boldsymbol{u} \in U\}} T. \tag{17}$$

We finally remark that, even though B-splines represent good approximations of feasible solutions, the possibility of finding the optimum is obviously related to the 'richness' of the search space. Given our particular choices, the only free variables in Algorithm 2 reduce to the total time T, as, together with the existing boundary conditions, this quantity completely specifies a candidate trajectory. However, we note that this fact is a consequence of having considered the smallest amount of control points for the B-spline in order to satisfy the given boundary conditions. Using B-splines (as any piecewise polynomial), it could be possible to introduce more degrees of freedom (i.e., more control points) without increasing the degree of each single polynomial. This would allow, in principle, to increase the dimension of the search space at will, but with a corresponding growth in complexity for the employed minimization algorithm.

V. SIMULATIONS

We conducted an extensive simulative study of our method. Both the general optimization in Algorithm 1 and the transfer trajectory optimization in Algorithm 2 have been solved using the Matlab Optimization Toolbox. Further details about the implementation can be found in [19]. The physical simulation of the robot dynamics and 3D rendering of the environment has been obtained using the SwarmSimX[5] simulation environment. In order to allow the quadrotor to track the planned trajectory in a robust way, we implemented the controller described in [23] in Matlab and used ROS as an interface between Matlab and SwarmSimX. We encourage the reader to watch the accompanying video where all the presented simulations can be fully appreciated.

In the first simulation reported in this paper, the robot starts and ends in hovering states with $\boldsymbol{r}_{\mathcal{B},i} = (0 \ 4 \ 3)^T$, $\boldsymbol{r}_{\mathcal{B},f} = (0 \ -4 \ 3)^T$ and $\psi_i = \psi_f = -\frac{3}{4}\pi$ During the gripper-closure phase, the target is at $\boldsymbol{r}_{\mathcal{T}} = (0 \ 0 \ 0.478)^T$ and moving along the $\boldsymbol{y}_{\mathcal{W}}$ axis at a constant velocity of 1 m/s. The initial guesses for the optimization variables have been chosen as $\zeta_g = \frac{\pi}{2}$, $\xi_g = \pi - \beta$, $\dot{\xi}_g = 0$, $T_g = T_g^{\min}$. Note that this corresponds to the case of a hovering gripper-closure trajectory. The optimization returned a solution very close to the initial guess both for the vertical and for the horizontal grasping trajectories. In these hovering conditions the two classes of trajectories coincide among themselves and with the final compound trajectory. If, instead, the optimization is started from a non-hovering initial guess for the gripper-closure trajectory (namely $\xi_g = \pi - \beta - 0.3$ for the horizontal grasping trajectory and $\xi_g = \pi - \beta - 0.1$ and $\dot{\xi}_g = -0.1$ for the vertical one), the optimization returns again values very close to the initial guess. However, while for the vertical grasping this results in a shorter trajectory duration, for the horizontal grasping the total time grows noticeably. This outcome is due to the presence of local minima in
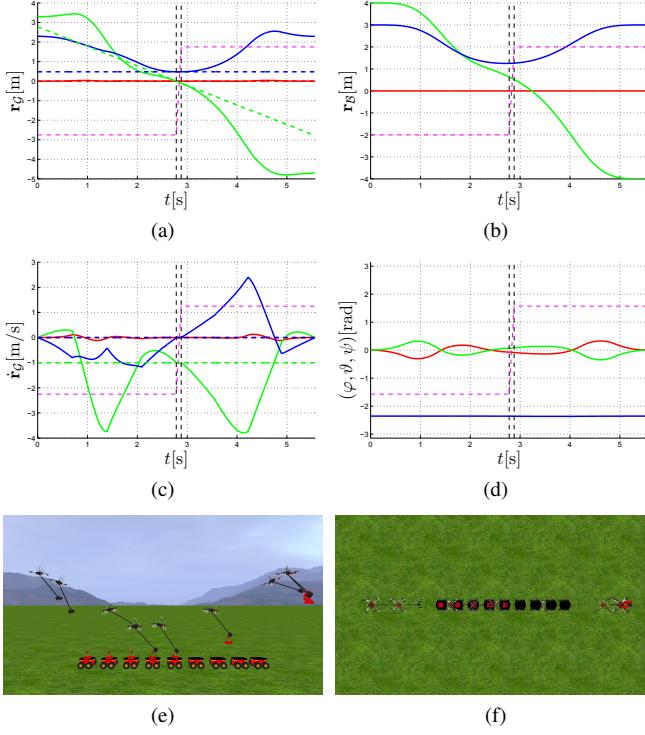
---
[5]http://laechele.eu/SwarmSimX/

Fig. 6: Vertical gripper-closure trajectory grasping: position (a) and velocity (c) of $O_{\mathcal{G}}$ (continuous line) and target (dashed line); position (b) and orientation (d) of the robot; stroboscopic lateral (e) and top (f) view of the simulation. The grasping interval is delimited by 2 vertical dashed lines. A magenta dashed line is superimposed to every plot, indicating the gripper state: from completely open (lower value) to completely closed (upper value).

Fig. 7: Horizontal gripper-closure trajectory grasping: position (a) and velocity (c) of $O_{\mathcal{G}}$ (continuous line) and target (dashed line); position (b) and orientation (d) of the robot; stroboscopic lateral (e) and top (f) view of the simulation. Grasping interval and gripper state are denoted as explained in Fig. 6.

the chosen cost function, thus preventing the gradient-based optimization routine to find the actual global optimum. The result for the vertical gripper-closure trajectory is reported in Fig. 6 where we can notice how the gripper is able to follow the target for the whole duration of the gripper-closure phase. By repeating the simulation for $\boldsymbol{r}_{\mathcal{B},i} = (-1; 4\ 3)^T$, $\psi_i = 0$ and $\boldsymbol{r}_{\mathcal{B},f} = (3\ -4\ 3)^T$, $\psi_f = \frac{\pi}{2}$, the optimization returns again a result close to the initial guess. However, in this case the horizontal trajectory is better (w.r.t. the completion time) than the vertical one. The resulting optimal trajectory is shown in Fig. 7.

Besides considering the task of grasping an object at some location in the world frame, our planning strategy can be seamlessly adapted to the case of a quadrotor initially carrying an object to be placed at some desired position. This idea can be also extended to the concatenation of multiple trajectories from the two considered classes by taking the final state of a trajectory as the initial state of the following one. Figure 8 presents the results of a concatenation of two pick-and-place operations using vertical gripper-closure trajectories. The targets are picked from and placed on some carriers independently moving in the environment. It is easy to note that during each grasping (placing) phase, delimited by blue vertical lines in the plots, the gripper tracks the same trajectory of one of the carriers present in the scene
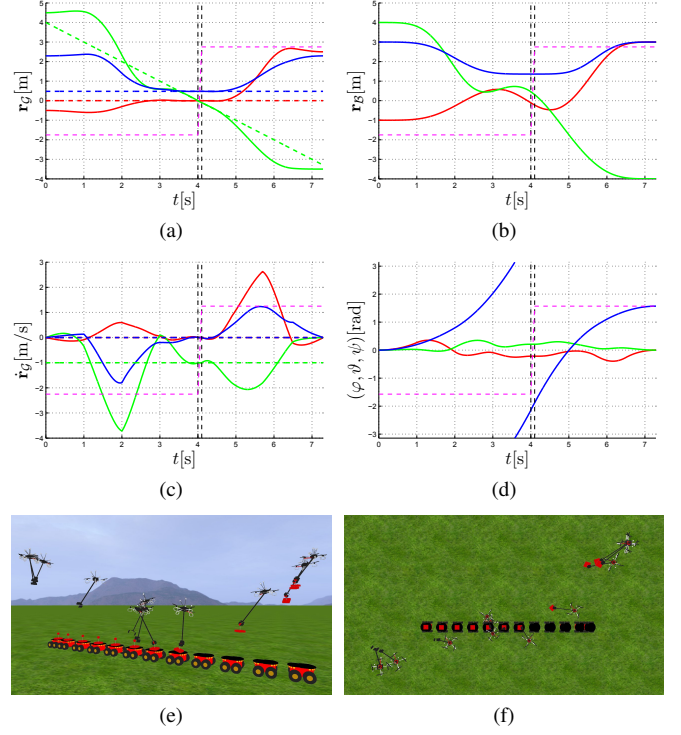
(represented by different dashed lines in the plots). Given the increased complexity in reporting the results of this last case, we again encourage the reader to watch the attached videoclip where the UAV motion can be fully appreciated.

VI. SUMMARY AND FUTURE WORKS

We presented a method for planning a time-optimal trajectory for a quadrotor equipped with an onboard gripper with the goal of grasping a moving target while traveling between generic initial and final states. We introduced and used two complementary set of trajectories able to continuously keep the quadrotor gripper in contact with the moving target. The method takes into account upper/lower bounds on the propeller speeds and the need of a finite time for the gripper in order to successfully perform the grasping task. Extensive physically-based simulations demonstrate the effectiveness of the proposed strategy.

Future works can exploit global search strategies with more degrees of freedom for the B-splines in order to tackle the non-convexity of the optimization problem and to obtain better solutions. We will also consider an unknown motion for the target together with a fast on-line re-planning based on the current measurement/estimation of the target motion. We also plan to augment the planning constraints in order to take into account limitations in the field of view of the robot sensors (e.g., cameras). Finally, we are currently working towards an experimental implementation of this method with
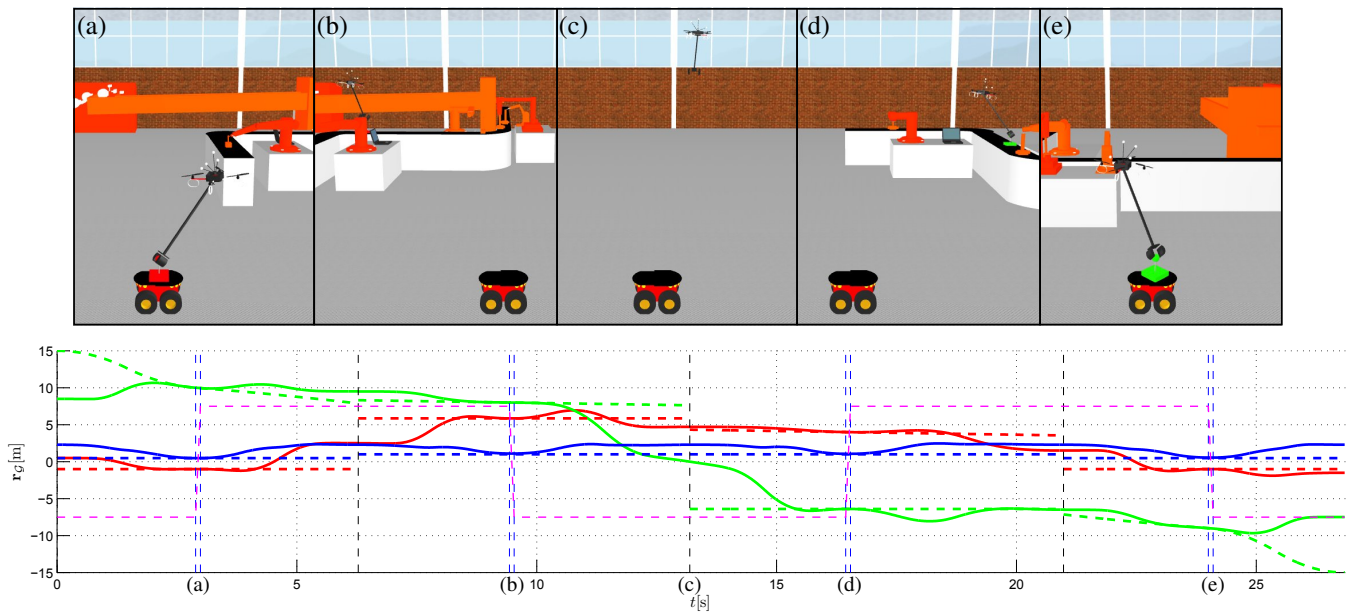
Fig. 8: Multiple pick-and-place operations: snapshots of the simulation; position of $O_\mathcal{G}$ (continuous line) and target carriers (dashed line). Grasping intervals and gripper state are denoted as explained in Fig. 6.

a real quadrotor UAV.

VII. ACKNOWLEDGMENTS

REFERENCES

[1] A. Franchi, C. Secchi, M. Ryll, H. H. Bülthoff, and P. Robuffo Giordano, "Shared control: Balancing autonomy and human assistance with a group of quadrotor UAVs." *IEEE Robotics & Automation Magazine*, vol. 19, no. 3, 2012.

[2] M. Schwager, B. Julian, M. Angermann, and D. Rus, "Eyes in the sky: Decentralized control for the deployment of robotic camera networks," *Proceedings of the IEEE*, vol. 99, no. 9, pp. 1541–1561, 2011.

[3] A. Franchi, C. Secchi, H. I. Son, H. H. Bülthoff, and P. Robuffo Giordano, "Bilateral teleoperation of groups of mobile robots with time-varying topology," *IEEE Trans. on Robotics*, In Press, Electronically published at http://ieeexplore.ieee.org/xpl/articleDetails.jsp?arnumber=6199993.

[4] P. Robuffo Giordano, A. Franchi, C. Secchi, and H. H. Bülthoff, "Passivity-based decentralized connectivity maintenance in the bilateral teleoperation of multiple UAVs," in *2011 Robotics: Science and Systems*, Los Angeles, CA, Jun. 2011.

[5] J. Fink, N. Michael, S. Kim, and V. Kumar, "Planning and control for cooperative manipulation and transportation with aerial robots," *International Journal of Robotics Research*, vol. 30, no. 3, pp. 324–334, 2010.

[6] D. Mellinger, M. Shomin, N. Michael, and V. Kumar, "Cooperative grasping and transport using multiple quadrotors," in *10th Int. Symp. on Distributed Autonomous Robotic Systems*, Lausanne, Switzerland, Nov. 2010.

[7] Q. Lindsey, D. Mellinger, and V. Kumar, "Construction of cubic structures with quadrotor teams," in *2011 Robotics: Science and Systems*, Los Angeles, CA, Jun. 2011.

[8] AIRobots, "EU Collaborative Project ICT-248669," www.airobots.eu.

[9] ARCAS, "EU Collaborative Project ICT-287617," www.arcas-project.eu.

[10] I. D. Cowling, J. F. Whidborne, and A. K. Cooke, "Optimal trajectory planning and LQR control for a quadrotor UAV," in *International Control Conference*, Glasgow, Scotland, Aug. 2006.

[11] Y. Bouktir, M. Haddad, and T. Chettibi, "Trajectory planning for a quadrotor helicopter," in *16th Mediterranean Conf. on Control and Automation*, Ajaccio, France, Jun. 2008, pp. 1258–1263.

[12] D. Mellinger and V. Kumar, "Minimum snap trajectory generation and control for quadrotors," in *2011 IEEE Int. Conf. on Robotics and Automation*, Shanghai, China, May. 2011, pp. 2520–2525.

[13] M. Hehn and R. D'Andrea, "Quadrocopter Trajectory Generation and Control," in *IFAC World Congress*, Milano, Italy, Sep. 2011, pp. 1485–1491.

[14] R. Ritz, M. Hehn, S. Lupashin, and R. D'Andrea, "Quadrocopter Performance Benchmarking Using Optimal Control," in *2011 IEEE/RSJ Int. Conf. on Intelligent Robots and Systems*, San Francisco, CA, Sep. 2011, pp. 5179–5186.

[15] D. Mellinger, N. Michael, and V. Kumar, "Trajectory generation and control for precise aggressive maneuvers with quadrotors," in *12th Int. Symp. on Experimental Robotics*, Delhi, India, Dec. 2010.

[16] D. Mellinger, Q. Lindsey, M. Shomin, and V. Kumar, "Design, modeling, estimation and control for aerial grasping and manipulation," in *2011 IEEE/RSJ Int. Conf. on Intelligent Robots and Systems*, San Francisco, CA, Sep. 2011, pp. 2668–2673.

[17] R. D'Andrea, F. Augugliaro, M. Corzillius, C. Flores, M. Hamer, M. Hehn, S. Lupashin, C. Male, M. Mueller, and I. Thommen, "Flying machine enabled construction," 2011. [Online]. Available: http://www.idsc.ethz.ch/Research_DAndrea/fmec

[18] V. Mistler, A. Benallegue, and N. K. M'Sirdi, "Exact linearization and noninteracting control of a 4 rotors helicopter via dynamic feedback," in *10th IEEE Int. Symp. on Robots and Human Interactive Communications*, Bordeaux, Paris, France, Sep. 2001, pp. 586–593.

[19] R. Spica, "Planning and control for aerial grasping with a quadrotor UAV," Master Thesis, DIAG, Università di Roma La Sapienza, 2012.

[20] M. Fliess, J. Lévine, P. Martin, and P. Rouchon, "Flatness and defect of nonlinear systems: Introductory theory and examples," *International Journal of Control*, vol. 61, no. 6, pp. 1327–1361, 1995.

[21] A. Isidori, *Nonlinear Control Systems, 3rd edition*. Springer, 1995.

[22] L. Biagiotti and C. Melchiorri, *Trajectory Planning for Automatic Machines and Robots*. Springer, 2008.

[23] T. Lee, M. Leokyand, and N. H. McClamroch, "Geometric tracking control of a quadrotor UAV on SE(3)," in *49th IEEE Conf. on Decision and Control*, Atlanta, GA, Dec. 2010, pp. 5420–5425.